Counter-diffusion biofilms have lower N2O emissions than co-diffusion biofilms during simultaneous nitrification and denitrification: Insights from depth-profile analysis

Kinh, Co Thi ; Suenaga, Toshikazu ; Hori, Tomoyuki ; Riya, Shohei ; Hosomi, Masaaki ; Smets, Barth F.; Terada, Akihiko

Published in:
Water Research

Link to article, DOI:
10.1016/j.watres.2017.07.058

Publication date:
2017

Document Version
Peer reviewed version

Graphical abstract

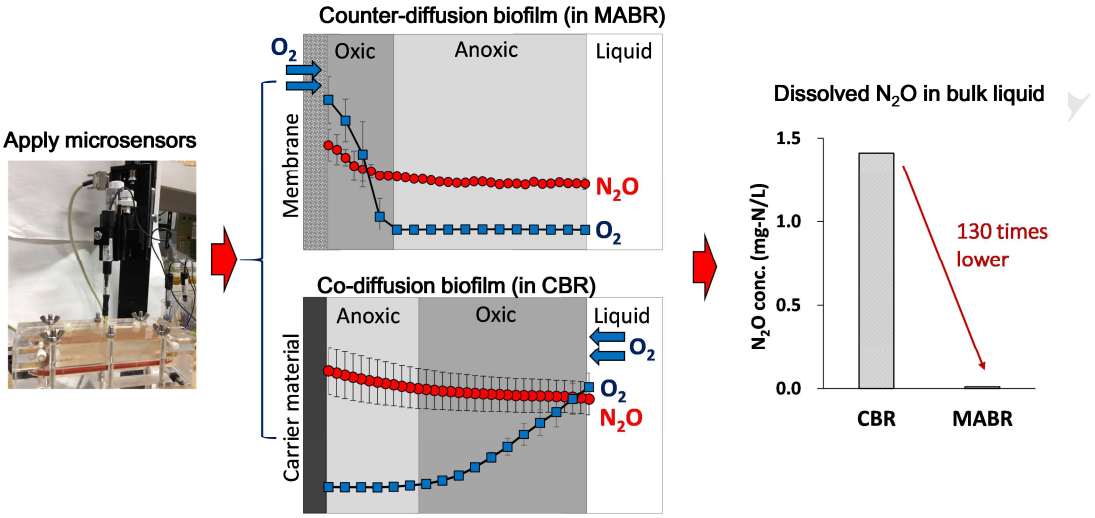

Counter-diffusion biofilms have lower N_2O emissions than co-diffusion biofilms during simultaneous nitrification and denitrification: Insights from depth-profile analysis

Co Thi Kinh[1], Toshikazu Suenaga[1], Tomoyuki Hori[2], Shohei Riya[1], Masaaki Hosomi[1], Barth F. Smets[3], Akihiko Terada*[1]

[1]Department of Chemical Engineering, Tokyo University of Agriculture and Technology, Naka 2-24-16 Koganei, Tokyo 184-8588, Japan

[2]Institute for Environmental Management Technology, National Institute of Advanced Industrial Science and Technology (AIST), Onogawa 16-1, Tsukuba, Ibaraki 305-8569, Japan

[3]Department of Environmental Engineering, Technical University of Denmark, Miljoevej, 2800 Lyngby, Denmark

Corresponding author: A. Terada (akte@cc.tuat.ac.jp)

Tel/Fax: +81-42-388-7069/+81-42-388-7731

Manuscript submitted to *Water Research*

Keywords: Nitrous oxide, Counter-diffusion biofilm, Microelectrode, Membrane-aerated biofilm reactor, Microbial community

ABSTRACT

The goal of this study was to investigate the effectiveness of a membrane-aerated biofilm reactor (MABR), a representative of counter-current substrate diffusion geometry, in mitigating nitrous oxide (N_2O) emission. Two laboratory-scale reactors with the same dimensions but distinct biofilm geometries, *i.e.*, a MABR and a conventional biofilm reactor (CBR) employing co-current substrate diffusion geometry, were operated to determine depth profiles of dissolved oxygen (DO), nitrous oxide (N_2O), functional gene abundance and microbial community structure. Surficial nitrogen removal rate was slightly higher in the MABR (11.0 ± 0.80 g-N/(m^2·day) than in the CBR (9.71 ± 0.94 g-N/(m^2·day), while total organic carbon removal efficiencies were comparable (96.9 ± 1.0% for MABR and 98.0 ± 0.8% for CBR). In stark contrast, the dissolved N_2O concentration in the MABR was two orders of magnitude lower (0.011 ± 0.001 mg N_2O-N/L) than that in the CBR (1.38 ± 0.25 mg N_2O-N/L), resulting in distinct N_2O emission factors (0.0058 ± 0.0005% in the MABR *vs.* 0.72 ± 0.13% in the CBR). Analysis on local net N_2O production and consumption rates unveiled that zones for N_2O production and consumption were adjacent in the MABR biofilm. Real-time quantitative PCR indicated higher abundance of denitrifying genes, especially nitrous oxide reductase (*nosZ*) genes, in the MABR versus the CBR. Analyses of the microbial community composition via 16S rRNA gene amplicon sequencing revealed the abundant presence of the genera *Thauera* (31.2 ± 11%), *Rhizobium* (10.9 ± 6.6%), *Stenotrophomonas* (6.8 ± 2.7%), *Sphingobacteria* (3.2 ± 1.1%) and *Brevundimonas* (2.5 ± 1.0%) as potential N_2O-reducing bacteria in the MABR.

1. Introduction

Nitrous oxide (N_2O) emission from biological wastewater treatment plants (WWTPs) is of considerable concern because of the extremely high global warming potential and contribution to ozone layer destruction by N_2O (Kampschreur et al. 2009, Law et al. 2012). Implementation of nitrogen-removing technologies, which can attain higher effluent quality and cost effectiveness, is expected to increase the N_2O emitted from biological WWTPs by approximately 13% between 2005 and 2020 (IPCC 2007, Itokawa et al. 2001, Okabe et al. 2011). It has been reported that the N_2O impact accounts for up to 78.4% of the total CO_2 footprint in WWTPs (Daelman et al. 2013). Therefore, mitigation of N_2O release from WWTPs is a key challenge.

N_2O is produced as a byproduct of nitrification and an intermediate of denitrification. Ammonia-oxidizing bacteria (AOB) or archaea produce N_2O via multiple pathways associated with nitrification and denitrification (Stein and Klotz 2011). Heterotrophic denitrifying bacteria likewise produce N_2O as a result of consecutive enzymatic reactions mediated by nitrate reductase, nitrite reductase and nitric oxide reductase (Morley and Baggs 2010, Philippot 2002, Robertson and Groffman 2015, Schreiber et al. 2012, Wrage et al. 2001, Wunderlin et al. 2012, Zumft 1997). The turnovers of these enzymes are determined by the limited supplies of oxygen for nitrification and of organic carbon for denitrification, affecting the amount of N_2O emission (Kampschreur et al. 2009). Therefore, mitigation strategies to suppress N_2O production have been implemented (Domingo-Félez et al. 2014, Rodriguez-Caballero et al. 2015).

Exploiting bacteria possessing nitrous oxide reductase (NosZ), also known as N_2O-reducing bacteria, as a N_2O sink is one mitigation strategy to reduce N_2O emissions from WWTPs (Desloover et al. 2012). The product of NosZ is N_2. Currently, N_2O-reducing bacteria are classified into two clades based on the amino acid sequences of NosZ (Jones et al. 2013, Sanford et al. 2012). Moreover, their physiological traits have been partially determined (Bueno et al. 2015, Desloover et

al. 2014, Yoon et al. 2016), extending their potential for application in mitigation of N_2O emissions. Nevertheless, it has been reported that NosZ is the most oxygen-sensitive of denitrifying enzymes (Bonin et al. 1992, Schulthess and Gujer 1996). Thus, provision of anoxic conditions and sufficient amounts of the electron donor and acceptor is of paramount importance in exerting the potential of N_2O-reducing bacteria.

Membrane-aerated biofilm reactors (MABR) could be a promising technology capable of enhancing N_2O mitigation. The reactor employs a fixed-film biological treatment technology where a substratum provides oxygen delivery and facilitates biofilm formation (Nerenberg 2016). Oxygen as an electron acceptor is supplied from the biofilm base without bubble formation, whereas electron donors are supplied from the biofilm exterior. Such counter-current substrate diffusion biofilm geometry, in theory, allows two contrasting environments where the electron donor concentration is highest and the oxygen concentration lowest at the biofilm-liquid boundary and *vice versa* at the biofilm-membrane boundary (**Figure S1A**). By utilizing this unique biofilm geometry, a MABR provides a niche in the middle of the biofilm where an electron acceptor co-exists with an electron donor without depletion of either. The niche created in the MABR allowed the occurrence of simultaneous nitrification/denitrification (SND) in a single reactor vessel (Cole et al. 2002, Downing and Nerenberg 2007, 2008b, LaPara et al. 2006, Semmens et al. 2003, Terada et al. 2003). The counter-current substrate diffusion geometry of MABR and its special biofilm niche, in conjunction with bubbleless aeration, could prevent N_2O exhaustion and thus facilitate N_2O mitigation. The mitigation effect has been previously demonstrated in a MABR introducing sequential aeration for partial nitrification (PN)-Anammox (Pellicer-Nacher et al. 2010). Nevertheless, *in situ* evidence of higher N_2O consumption activity has not been obtained in a MABR biofilm.

Here, we provide proof of the concept that a MABR for SND can mitigate N_2O emissions. To

this end, reactor operation and *in situ* biofilm depth investigation were conducted to reveal: (i) whether a MABR with counter-diffusion biofilm geometry allows the lower amount of N_2O emitted than a conventional biofilm reactor (CBR) with co-diffusion biofilm geometry; (ii) how the spatial distributions of the abundance and activity of N_2O-reducing bacteria vary within the biofilms; and (iii) whether the microbial community structure in the counter-diffusion biofilm is distinct depending on the biofilm depth. To address these research questions, we combined microelectrodes with molecular microbiological methods, *i.e.* quantitative PCR and high-throughput sequencing technology of 16S rRNA gene amplicons, to compare the counter- and co-diffusion biofilms.

2. Materials and methods

2.1. Reactor setup

Two laboratory-scale flow-cell reactors employing counter- and co-diffusion biofilm geometries, a membrane-aerated biofilm reactor (MABR) and a conventional biofilm reactor (CBR) respectively, were operated for 95 days. Each reactor consisted of liquid and gaseous compartments, between which a gas-permeable flat-type silicone membrane (Rubber Co., Tempe, AZ, USA) was inserted. The silicon membrane was 1,000 µm thick and its surface area in each reactor was 41.5 cm^2. The liquid compartment of each reactor had an effective volume of 0.2 L (specific surface area of the silicone membrane of 20.8 m^2/m^3). The dimensions of both reactors were identical, except that the CBR had a non-permeable plate beneath the silicone membrane (**Figure S2B**). Air was supplied into the two reactors by an air pump (Hiblow, HP100, Saline, MI, USA) with a flow controller. As the entry for oxygen, a bundle of 96 hollow-fibers (MHF3504; Mitsubishi Rayon Co., Ltd., Tokyo, Japan) as a gas permeable membrane was suspended in the liquid phase in the CBR. Whereas the CBR received air via the fiber bundle at an applied pressure of 15 kPa and an air-flow rate of 20

mL/min, the MABR received air from the gas compartment (volume 20 mL) via the silicone membrane at 7 kPa and 20 mL/min (**Figure S2A**). Aeration conditions were set based on the preliminary oxygen mass transfer rate estimations (Ahmed et al. 2004). Based on preliminary oxygen transfer tests (data not shown), these conditions provided a comparable oxygen loading rate to the biofilms in the MABR and CBR. The top of both reactors possessed three ports in which microelectrodes were inserted to measure the dissolved N_2O and O_2 concentrations in the biofilms. Synthetic medium, mimicking food-processing wastewater, consisted of CH_3COONa (0.65 g/L), $(NH_4)_2SO_4$ (0.90 g/L) and 100 mL/L of mineral solution comprised of (in mg/L): $MgSO_4 \cdot 7H_2O$ (280), KH_2PO_4 (27), $CaCl_2 \cdot 2H_2O$ (120), NaCl (600), $FeSO_4 \cdot 7H_2O$ (3.3), $MnSO_4 \cdot H_2O$ (3.3), $CuCl_2 \cdot 2H_2O$ (0.8), $ZnSO_4 \cdot 7H_2O$ (1.7), and $NiSO_4 \cdot 6H_2O$ (0.3). The medium was sterilized prior to use. The synthetic medium was continuously supplied at 13.8 mL/h by a peristaltic pump (ISMATEC, ISM 930, Wertheim, Germany), ensuring a hydraulic retention time of 14.5 h. Complete mixing was accomplished by a recirculation pump (Masterflex 7553-50, Tokyo, Japan), providing an effective flow rate of 42 mL/s. Effluent samples were collected every few days to evaluate the reactor performances. The fiber bundle in the CBR was cleaned weekly to prevent biofilm growth, so as to maintain constant oxygen supply to the biofilm on the silicone membrane.

2.2. Reactor operation

The two biofilm reactors, *i.e.* the MABR and CBR, were inoculated from a laboratory-scale sequencing batch reactor for partial nitrification (Terada et al. 2013). The inoculum was recirculated in the reactors for 3 days to facilitate bacterial adhesion and biofilm formation. Subsequently, the reactors were fed with synthetic wastewater containing dissolved organic carbon (DOC) and ammonium at concentrations of 190 mg-C/L and 190 mg-N/L, respectively. This condition allowed specific DOC and nitrogen loading rates of 15.1 g-C/(m^2·day) and 15.1 g-N/(m^2·day), respectively. The temperature was kept at 30°C. pH of the reactors were controlled at 7.0 by addition of $NaHCO_3$.

Because denitrification produces alkalinity, which offsets acidity produced via nitrification (Tenno et al. 2016), additional pH control was not necessary. Instead, pH monitoring at every sampling time was carried out in order to verify neutral pH condition in the reactors (7.0 ± 0.2).

2.3. Chemical analysis of influent and effluent wastewater

A sample was filtered through a 0.45-μm pore size membrane (DISMIC-13HP045AN; Advantec, Tokyo, Japan). DOC and total dissolved nitrogen (TDN) concentrations were measured by a TOC analyzer (TOC 5000A, Shimadzu, Kyoto, Japan). Nitrate (NO_3^-), nitrite (NO_2^-) and ammonium (NH_4^+) concentrations were measured using a flow injection analyzer (PE-230, Human Manufacture Engineering, Japan). *t*-test was employed in SPSS 13.0 (IBM Co., New York, USA) to compare DOC and dissolved nitrogen concentrations in the effluents of the two reactors. Dissolved N_2O concentration was measured using a Clark-type microelectrode (Unisense, Aarhus, Denmark). The N_2O emission factor was estimated as the ratio of dissolved N_2O concentration in the bulk liquid to the influent TDN concentration. This factor assumes negligible N_2O exhaustion to the gas phase due to bubbleless aeration, which was confirmed from the gaseous N_2O concentration in the ports for microelectrode insertion, in the gas compartment of the MABR, and in lumens of the hollow-fibers in the CBR.

2.4. Measurement of dissolved O_2 and N_2O concentrations in biofilms

Dissolved N_2O and dissolved oxygen (DO) concentrations throughout the depth of the biofilms were measured using Clark-type microelectrodes (Unisense, Aarhus, Denmark), connected to a picoammeter (MM 3 Microsensor Multimeter, Unisense, Aarhus, Denmark) for data acquisition (Lackner et al. 2010). The diameters of DO and N_2O microelectrodes were 50 μm and 25 μm, respectively. Calibration of each microelectrode was performed prior to the application to a biofilm according to a previous report (Schreiber et al. 2009). The micromanipulator and microelectrodes

were precisely controlled using Sensor Trace Pro software (Unisense, Aarhus, Denmark). Biofilm thicknesses were measured by oxygen concentration profiles. The biofilm depth profiles of N_2O and O_2 concentrations were acquired at 10–15 points from the middle port for microelectrode insertion on days 90 and 95 of reactor operation. The average net volumetric N_2O consumption/production rates by biofilm volume were estimated and averaged from each concentration profile using Fick's second law of diffusion, assuming steady-state conditions (Lorenzen et al. 1999).

2.5. Biomass sectioning

On day 95, each biofilm (approximately 1500 μm thickness) was cut by a scalpel to 0.6 × 0.6 cm and transferred onto a Petri dish with the orientation maintained, as previously described (Terada et al. 2010). Each biofilm was embedded in optimum cutting temperature compound (Tissue-Tek OCT compound, Miles, Elkhart, Ind., IN, USA) overnight to infiltrate the OCT compound into the biofilm, and subsequently frozen at -20°C. The frozen biofilms were horizontally cut into 100 μm-thick sections with a cryomicrotome (Cryocut 1800; Leica, Mannheim, Germany) at -20°C and transferred in 1.5-mL microtubes for ensuing DNA extraction.

2.6. DNA extraction, real time PCR, and next generation sequencing by Illumina MiSeq™

DNA extraction was processed using a Fast DNA™ Spin Kit (FastDNA Spin Kit for Soil, MP-Biomedicals, Santa Ana, CA, USA) per the manufacturer's protocol, followed by measurement of DNA concentrations using a spectrophotometer (NanoDrop 2000c, Thermo Scientific, Wilmington, DE, USA). Abundances of functional genes encoding ammonia monooxygenase (bacterial *amoA*), copper and cytochrome cd_1-type nitrite reductases (*nirK* and *nirS* respectively), and N_2O reductase (clade I and clade II type *nosZ*) were quantified by real-time quantitative PCR (qPCR) (CFX96 Touch™ Real-Time PCR Detection System, BioRad Laboratories, Hercules, CA, USA). The details of the qPCR procedures are given in Supplementary Information. The PCR

conditions were the same as used in previous work (Song et al. 2015).

High-throughput sequencing based on 16S rRNA gene amplicons was performed on an Illumina MiSeq platform. The V4 region of 16S rRNA genes was amplified using the primer set 515f–806r and the obtained amplicon was subjected to analysis according to the detailed protocol described elsewhere (Aoyagi et al. 2015, Itoh et al. 2014, Schloss et al. 2009) (Supplementary Information). Operational taxonomic units (OTUs) were defined using a threshold of 97% identity. Alpha and beta diversities were calculated by the software QIIME (Caporaso et al. 2010). Principal coordinate analysis was performed based on weighted UniFrac analysis. The sequence data acquired in this study have been deposited in the MG-RAST database (http://metagenomics.anl.gov/) named "Counter-diffusion and co-diffusion biofilm for simultaneous nitrification and denitrification reduces N_2O emission" under project ID PSUB006788.

3. Results

3.1. Carbon and nitrogen removal performances of the MABR and CBR

Time courses of DOC and nitrogen concentrations are shown in **Figure S3**. According to the trends, the MABR and CBR achieved steady-state performances by day 43 (**Figure S3**). The average effluent concentrations of DOC, TDN, NH_4^+, NO_2^-, and NO_3^- after day 43 are summarized in **Figure 1**. The average effluent TDN concentration was lower in the MABR (53.7 ± 9.2 mg-N/L) than in the CBR (70.0 ± 10.7 mg-N/L, $p = 5.4 \times 10^{-6}$). Nitrogen removal efficiency was higher in the MABR (72.0 ± 4.8%) than in the CBR (63.5 ± 5.6%, $p = 1.6 \times 10^{-4}$), resulting in specific nitrogen removal rates of 11.0 ± 0.80 and 9.71 ± 0.94 g-N/(m^2·day) for the MABR and CBR, respectively. Average effluent DOC concentrations in the two reactors were different, *i.e.*, 5.8 ± 1.8 mg/L in the MABR and 3.7 ± 1.5 mg/L in the CBR ($p = 7.0 \times 10^{-3}$). DOC removal performances of

the MABR and CBR were both high, at 96.9 ± 1.0% and 98.0 ± 0.8%, equivalent to specific DOC removal rates of 14.8 ± 0.39 and 15.0 ± 0.38 g-C/(m^2·day) for the MABR and the CBR, respectively.

3.2. Depth-profile of DO concentration in biofilms

The depth profiles of DO concentrations in the MABR and CBR on day 95 are shown in **Figures 2A** and **2B**. On day 95, the TDN concentrations in the MABR and CBR were 39.5 and 72.6 mg-N/L, respectively, showing the superior nitrogen removal by the MABR. The biofilm thicknesses were 1400 ± 200 μm in the MABR and 1500 ± 200 μm in the CBR. The DO penetration depth in the MABR (ca. 300 μm) was shallower than that in the CBR (ca. 800 μm), indicating a steep gradient occurred in the MABR biofilm. In the MABR, the DO concentration was highest (2.25 ± 0.5 mg/L) at the biofilm-membrane interface (0 μm) where air was supplied (**Figure 2A**). In contrast, in the CBR, the DO concentration was higher at the outermost biofilm surface (1.17 ± 0.22 mg/L) and decreased to 0 mg/L at 600 μm from the biofilm-membrane interface (**Figure 2B**).

3.3. Depth-profile of N_2O concentration in biofilms

The gaseous N_2O concentrations in the gas compartment of the MABR and the lumens of the hollow-fiber bundle in the CBR were not distinguishable from the ambient atmospheric N_2O concentrations, indicating negligible levels of N_2O diffusion into the gas compartment (data not shown). N_2O concentration profiles and net volumetric N_2O consumption/production rates in the MABR and CBR are shown in **Figures 2C** and **2D**. The dissolved N_2O concentration at the biofilm-liquid interface in the MABR (0.011 ± 0.001 mg N_2O-N/L) was 130-times lower than that in the CBR (1.38 ± 0.25 mg N_2O-N/L). In the CBR, the highest and lowest N_2O concentrations

were respectively detected in the innermost (1.77 ± 0.37 mg N_2O-N/L) and outermost parts (1.39 ± 0.25 mg N_2O-N/L) of the biofilm.

The depth profile of the net N_2O consumption/production rate in the MABR indicated that N_2O production mainly occurred from 0 to 200 μm from the biofilm bottom (the biofilm-membrane interface), at rates of 0.0021–0.0043 mg-N/cm^3/h varying with biofilm depth. On the contrary, the highest net N_2O consumption rate was observed 250–450 μm from the biofilm bottom, at a rate of 0.0051 mg-N/cm^3/h (**Figure 2C**). In the CBR biofilm, the highest N_2O production was observed in the outermost regions (1300–1500 μm from the biofilm bottom) with the highest rate of 0.034 mg-N/cm^3/h. In contrast, N_2O consumption was broadly distributed from 0 to 900 μm, with a rate of 0.002–0.02 mg-N/cm^3/h. The highest N_2O consumption rate in the CBR was 0.026 mg-N/cm^3/h at 500 μm from the biofilm bottom, 5.1 times as high as that in the MABR (0.0051 mg-N/cm^3/h). In summary, the MABR biofilm exhibited a lower net N_2O production/consumption rate within a narrower region than the CBR.

3.4. Depth profile of functional gene abundances in biofilms

The depth profiles of the abundances of functional genes for ammonia oxidation (bacterial *amoA*) and denitrification (*nirK*, *nirS*, and clade I/clade II type *nosZ*) in the MABR and CBR are shown in **Figure 3**. The copy numbers of archaeal *amoA* genes were below the detection limit at all locations (<10^2 copies/ng-DNA) (data not shown). The abundance of bacterial *amoA* genes in the MABR was generally comparable to that in the CBR: the copy numbers of bacterial *amoA* genes ranged from 2.7–7.3×10^6 copies/ng-DNA in the MABR and from 3.2×10^6–1.1×10^7 copies/ng-DNA in the CBR. In the MABR, the *amoA* gene abundance was higher in the biofilm interior than in the biofilm exterior by a maximum factor of 2.7 (**Figure 3A**). The opposite trend was obtained in the CBR, where bacterial *amoA* gene abundance was higher in the exterior than in the interior of the biofilm, by a maximum factor of 3.4 (**Figure 3B**).

In both the biofilms, *nirK* gene copy numbers were the highest among the examined functional genes, in the order of 10^8 copies/ng-DNA. The *nirK* depth profile in the MABR was irregular, whereas the copy number in the CBR was higher deeper in the biofilm than in the outer (surface) layers (**Figure 3C, D**). The abundance of *nirS* genes was comparable between the MABR and CBR. The trends of *nirS* gene distribution were similar to those of *amoA* genes, *i.e.*, higher *nirS* gene copy numbers were found close to the biofilm bottom in the MABR and at the outermost surface of the biofilm in the CBR (**Figure 3A, B**).

The depth profiles of clade I and clade II *nosZ* genes were more pronouncedly stratified in the MABR biofilm than in the CBR biofilm. The abundances of clade I *nosZ* genes at 200–600 μm in the MABR biofilm were higher ($3.3–4.4\times10^6$ copies/ng-DNA) than those in other parts of the biofilm ($1.6–3.3\times10^6$ copies/ng-DNA) (**Figure 3A**). In the CBR, the abundances of clade I *nosZ* genes were relatively constant throughout the biofilm depth, ranging from 1.7×10^6 to 3.1×10^6 copies/ng-DNA (**Figure 3B**). The abundances of clade II *nosZ* genes increased by a factor of two from the bottom (0.96×10^5 copies/ng-DNA) to 200 μm (1.9×10^5 copies/ng-DNA) in the MABR biofilm and remained constant with distance above 200 μm (**Figure 3C**). The opposite trend was apparent for clade II *nosZ* gene abundance in the CBR biofilm, *i.e.* decreasing abundance with distance from the biofilm bottom (**Figure 3D**).

3.5. Microbial community structure in the biofilms by Illumina MiSeq sequencing

Alpha-diversities of the MABR and CBR biofilms were comparable and no substantial changes in these diversities were observed within either biofilm (**Table S1**, **Figures S4** and **S5**. For details, see Supplementary Information). **Figure 4** shows the bacterial community composition at the OTU level throughout the biofilm depth. The highly abundant OTUs were identical in the MABR and CBR. However, the relative abundance differed by biofilm depths in the MABR and CBR. The most abundant OTU in both the biofilms was identical to *Thauera mechernichensis* (denovo 33439)

of the family Rhodocyclaceae, accounting for 31.2 ± 11% and 30.3 ± 4.3% of the total read numbers in the MABR and CBR, respectively. This OTU was especially high in abundance from 0–800 µm in the MABR biofilm, while far less dynamic stratification was observed in the CBR. The second most abundant OTU was *Rhizobium* sp. (denovo 24831) with abundance in the MABR (10.9 ± 6.6%) slightly higher than that in the CBR (5.2 ± 1.2%). The third to fifth most abundant OTUs were *Stenotrophomonas nitritireducens* (denovo 3270) (6.8 ± 2.7% *vs.* 3.2 ± 1.5% in the MABR and CBR respectively), *Sphingobacteria* (denovo 25291) (3.2 ± 1.1% *vs.* 2.9 ± 0.4% in the MABR and CBR respectively), and *Brevundimonas diminuta* (denovo 11916) (2.5 ± 1.0% *vs.* 0.4 ± 0.5% in the MABR and CBR respectively).

A singular AOB, *Nitrosomonas* (denovo 28142), was distributed across the biofilm depth in both systems with relative abundances in the MABR and CBR ranging from 1.5–3.1% and 2.2–5.5%, respectively (**Figure 4**). The abundance of this OTU in both the biofilms decreased after the inoculation; the abundance in the inoculum was 13.7% (**Figure S6**). Far lower abundances of nitrite-oxidizing bacteria (NOB) than AOB were detected in both the MABR and CBR. In addition, no clear spatial distribution of the NOB abundances was observed in either biofilm (**Figure S7**). All the NOB detected were affiliated to *Nitrobacter* spp., and not *Nitrospira* spp.

4. Discussion

4.1. Far less N_2O emission in the MABR than in the CBR

This is the first comprehensive study demonstrating that a MABR emitted far less N_2O than a CBR under operational conditions that give comparative nitrogen removal rates via nitrification/denitrification (**Figures 1** and **2**). After stable operation the reactors since 50 days (**Figure S3**), depth-profiles of O_2, N_2O and the microbial community structure were determined in both biofilms. The superior TDN removal efficiency obtained in the MABR (**Figure 1** and **S3**)

underscores that a MABR is suitable to achieve SND (Cole et al. 2004, Downing and Nerenberg 2007, LaPara et al. 2006, Nerenberg 2016, Syron and Casey 2008, Terada et al. 2003). The surficial TDN removal rate was 11.0 ± 0.80 g-N/(m^2·day) with the removal efficiency of 72.0 ± 4.8% in the MABR, higher than those of previous reports (1.5 to 9.3 g-N/(m^2·day)) with the removal efficiencies of 70-85% (Brindle et al. 1998, Downing and Nerenberg 2008a, Hsieh et al. 2002, Liu et al. 2007, Semmens et al. 2003, Suzuki et al. 2000, Syron et al. 2015, Terada et al. 2003, Walter et al. 2005), likely due to oxygen permeability of the membrane and homogenous biofilm formation onto a planar surface (note that the membrane was a flat-sheet). Here, we show an additional benefit of the MABR, *i.e.*, mitigation of N_2O emission. A N_2O concentration two orders of magnitude lower was observed in the bulk liquid in the MABR compared with the CBR (**Figure 2**). Assuming negligible N_2O exhaustion to the gas phase (note that the aeration mode was bubbleless), N_2O emission factors over the TDN load of the MABR and CBR were 0.0058 ± 0.0005% and 0.72 ± 0.13%, respectively. While N_2O emission factors have been inconsistently defined, the value in the MABR was much lower than those in previous SND processes, *e.g.*, a hybrid sequencing batch reactor (21% of the nitrogen load) (Lo et al. 2010), a trickling filter system under hypoxia (0.4% of the influent NH_4^+ load), and stoichiometrically modest methanol-fed conditions (0.2% of the NO_3^- load) (Tallec et al. 2006a). The results of our study agree with previous observation of a PN-Anammox MABR, where <0.015% N_2O conversion was noted (Pellicer-Nacher et al. 2010). Nevertheless, we provide the first head-to-head comparison of a CBR with a MABR operated with identical influent loading, with only the biofilm geometry different, which evidences that the MABR is advantageous over the CBR to reduce N_2O emissions.

The far lower N_2O emission from the MABR is likely due to the optimal relative positions of the N_2O production and consumption zones. As **Figure 2C** shows, the hot spots for N_2O production and consumption were at depths of 0–200 and 250–450 μm, respectively. Given that the region for N_2O

production roughly coincided with the oxygen penetration depth (**Figure 2A** and **C**), N_2O was likely produced by AOB, and was immediately reduced to N_2 adjacent to the aerobic zone. N_2O production and consumption rates appeared irregular from 500 to 1400 μm in the MABR, plausibly due to the co-occurrence of N_2O production and consumption mediated by denitrifying bacteria with high turnovers of the consecutive denitrification reactions (note that the values in **Figures 2C** and **2D** are net, rather than absolute). The exterior in a counter-diffusion biofilm for SND confers favorable conditions for denitrification because the DOC is high but oxygen is absent (Matsumoto et al. 2007). This supports our hypothesis on the high denitrification turnover in the biofilm exterior. Taken together, the adjacent positioning of the zones for N_2O production/consumption and the favorable conditions at the biofilm exterior (higher DOC and lower DO concentrations) accelerate N_2O consumption in the MABR biofilm, resulting in the advantage of this reactor in N_2O mitigation.

The broader oxygen penetration depth and segregation of the hotspots for N_2O production and consumption may result in higher N_2O production in the CBR (**Figure 2B** and **D)**. Reportedly, a low DO concentration for nitrification and insufficient organic carbon supply for denitrification stimulate N_2O production (Desloover et al. 2012, Kampschreur et al. 2009, Law et al. 2012). Given that DO concentrations were <1 mg/L in a large part of the CBR biofilm (0.01–0.82 mg/L from 0–1400 μm), these hypoxic conditions potentially facilitate N_2O emission from the CBR (Peng et al. 2014, Tallec et al. 2006a, Tallec et al. 2006b). In addition to the N_2O production in the broad hypoxic zone, N_2O consumption was observed at 0 to 500 μm (**Figure 2D**). The distance between the hotspots for N_2O production and consumption is disadvantageous because the long distance required for DOC diffusion in the deeper biofilm acts as mass transfer resistance. In co-diffusion biofilms, the highest DOC and oxygen concentrations are found at the uppermost biofilm surface, limiting the DOC available for anoxic respiration including N_2O reduction (Matsumoto et al. 2007).

Therefore, the lower DOC concentration in the deeper biofilm of the CBR likely limits N_2O consumption, leading to N_2O accumulation.

Another reason for the large difference in the bulk liquid N_2O concentrations could be the difference in DO concentrations at the innermost (2.25 mg/L in **Figure 2C**) and outermost biofilms (1.17 mg/L in **Figure 2D**) in the MABR and CBR. The DO difference was inevitable at the same oxygen loading in both reactors because the CBR forced oxygen to be penetrated through the boundary layer to the biofilm. Ideally, N_2O production in the MABR and CBR should be compared with the same DO concentration at the bottom and top of the respective biofilms. Furthermore, the N_2O production mechanisms and the effects of operational conditions, e.g. pH, temperature, aeration regimes, and DOC/TDN loading rates, on N_2O emission need to be performed in future.

4.2. N_2O reducers in biofilms for SND

Irrespective of the biofilm geometries, *Thauera mechernichensis* was predominant in both the biofilms (**Figure 4**). Despite the lack of genomic information on *T. mechernichensis* so far, it has been reported that *T. mechernichensis* is a canonical denitrifier capable of reducing NO_3^- to N_2 via N_2O (Scholten et al. 1999), as demonstrated by other *Thauera* species (Liu et al. 2013), and is present in an nitrogen-removing bioreactor for industrial wastewater treatment (Chang et al. 2011). Given the N_2O consumption potential, *T. mechernichensis* likely reduced N_2O to N_2 at the region from 200 to 300 μm in the MABR biofilm, where N_2O consumption intensively occurred (**Figure 2C**). Furthermore, this species reportedly reduces NO_3^- and NO_2^- even at high DO concentrations (Scholten et al. 1999), also confirmed by other species phylogenetically close to *Thauera* species (Liu et al. 2013, Yokoyama et al. 2016). The high abundance of *T. mechernichensis* across a large section of the biofilms, especially from 100–800 μm in the MABR biofilm, suggests its high contribution to denitrification and N_2O consumption. *Rhizobium*, detected in high abundance in the MABR, is also a canonical denitrifier, present in activated sludge, soil, and freshwater environments

(Jones et al. 2008, Rochette and Janzen 2005, Wang et al. 2014, Zhao et al. 2013), and most species of the genus *Rhizobium* carry *nosZ* (Rochette and Janzen 2005). Interestingly, the *Rhizobium* OTUs were more abundant in the MABR biofilm exterior than in the interior (**Figure 4A**) and, in contrast, these OTUs were less abundant in the CBR than in the MABR (**Figure 4B**). The physiology of the genus *Rhizobium* remains unclear; however, the higher abundance of this genus in the MABR than in the CBR may be responsible for the greater N_2O consumption of the former, plausibly causing the stark contrast in N_2O emission. Additionally, *Stenotrophomonas nitritireducens* (6.8 ± 2.7% on average in samples from the MABR) and *Brevundimonas diminuta* are known N_2O reducers (Finkmann et al. 2000) previously detected in wastewater treatment bioreactors (Chèneby et al. 1998, Schweitzer et al. 2001, Srinandan et al. 2011, Yu et al. 2008). Moreover, the *Sphingobacteria* OTU (family Chitinophagaceae) is another denitrifier present in both biofilms (Gabarro et al. 2013, Pan et al. 2013). While more thorough *in situ* analysis on profiles of electron donors and acceptors would be warranted, the better environmental conditions, i.e. the close positions for nitrification and denitrification discussed in *4.1* and the inherent geometry of counter-diffusion biofilm as shown in **Figure S1**, likely facilitated the growth of more abundant potential N_2O-reducing bacteria in the MABR than in the CBR biofilm.

4.3. Implications of functional gene profiles for N_2O reduction

Irrespective of the biofilms in the MABR and CBR, the aerobic regions, as shown in **Figure 2**, showed higher abundances of *amoA* genes than the anoxic zones. The trend was consistent with the depth profiles of *amoA* genes (Cole et al. 2004, LaPara et al. 2006) and the 16S rRNA genes of AOB (Terada et al. 2010) in counter-diffusion biofilms. The relatively higher abundances of clade I and clade II *nosZ* genes in the anoxic regions (300–600 μm and 300–1400 μm, respectively) than in the aerobic part in the MABR biofilm (**Figure 3A** and **C**) indicate that the microaerophilic (0-300 μm) and anoxic regions (300 μm-) likely favored the growth of N_2O-reducing bacteria. The absence

of DO and corresponding high gene abundances were likewise observed for clade II *nosZ* in the deeper part of the CBR biofilm (**Figure 3D**), but not for clade I *nosZ* (**Figure 3B**). The reason for the incongruence of redox-conditions and gene abundance for clade I *nosZ* could be the limited supply of organic carbon in the influent (C/N ratio = 1) and the inherent geometry of a co-diffusion biofilm, which consumes organic carbon coupled with oxygen respiration. Reportedly, a MABR allows denitrifying bacteria to effectively utilize organic carbon and nitrogen oxides in the middle part of the biofilm (Cole et al. 2004, LaPara et al. 2006). This results in more pronounced gene profiles of clade I *nosZ* genes. Because biokinetic information of N_2O-reducing bacteria is still limited, reasons for selective growth of the N_2O reducers in the anoxic parts of the CBR biofilm entail further investigations.

Summarizing these depth profiles of functional genes, redox zonation created in the MABR biofilm permitted more dynamic distribution of AOB and N_2O-reducing bacteria than was found in the CBR biofilm. The closer association of regions for N_2O production and consumption in the MABR biofilm (**Figure 2C**) likely facilitated relay of N_2O plausibly produced by AOB to N_2O-reducing bacteria adjacent to the AOB. This adjacency of these potential N_2O producers and consumers allowed the latter to consume N_2O, resulting in lower N_2O emissions from the MABR. To consolidate this concept, transcription levels of these functional genes, reflecting activities by biofilm depth, and visualization of AOB and N_2O-reducing bacteria in a biofilm, warrant future study.

5. Conclusions

To the best of our knowledge, this is the first report directly comparing a MABR and CBR in terms of overall and spatially resolved N_2O production/reduction and microbial community composition as a function of biofilm depth. The two biofilms, employing counter- and co-current substrate

diffusion geometries respectively, were supplied with a high nitrogen-containing wastewater with low DOC/TDN ratio of 1.0 at the same loading rate, and performed simultaneous nitrification and denitrification.

- TDN removal efficiency (72.0 ± 4.8%) was higher in the MABR than in the CBR (63.5 ± 5.6%).
- Dissolved N_2O concentrations were two orders of magnitude lower in the MABR than in the CBR.
- N_2O emission factors of the MABR and CBR, normalized to TDN load, were 0.0058 ± 0.0005% and 0.72 ± 0.13%, respectively.
- The MABR biofilm had narrower regions for N_2O production and consumption than the CBR biofilm.
- Higher abundances of denitrifying genes, especially *nosZ*, were observed in the MABR than in the CBR.
- Microbial community structure revealed the presence of OTUs affiliated within the genera *Thauera*, *Rhizobium*, *Stenotrophomonas*, *Sphingobacteria* and *Brevundimonas* as potential N_2O-reducing bacteria with higher abundances in the MABR biofilm than in the CBR biofilm.

Taking these findings into account, MABRs promise a small-footprint technology achieving both effective simultaneous nitrification/denitrification and mitigation of N_2O emissions.

ACKNOWLEDGEMENTS

We acknowledge Ms. Kanako Mori, Dr. Tomo Aoyagi, Dr. Hirotsugu Fujitan and Prof. Satoshi

Tsuneda for technical support in 16S rRNA gene amplicon sequencing and cryosectioning of biofilm samples. This work was supported by a Grant-in-Aid for Scientific Research for Young Scientists (A) (26701009), a Grant-in-Aid for Challenging Exploratory Research (16K12616), a Grand-in-Aid for JSPS Fellows (16J08490) of the Ministry of Education, Culture, Sports, Science and Technology, Japan, the Open Partnership Joint Research Projects (Japan-Denmark) from the Japan Society for the Promotion of Science (JSPS), and the Danish Free Research Council (N2OMAN grant no. DFF-1335-00100).

REFERENCES

Ahmed, T., Semmens, M.J. and Voss, M.A. (2004) Oxygen transfer characteristics of hollow-fiber, composite membranes. Adv Environ Res 8(3-4), 637-646.

Aoyagi, T., Hanada, S., Itoh, H., Sato, Y., Ogata, A., Friedrich, M.W., Kikuchi, Y. and Hori, T. (2015) Ultra-high-sensitivity stable-isotope probing of rRNA by high-throughput sequencing of isopycnic centrifugation gradients. Environ Microbiol Rep. 7(2), 282-287.

Bonin, P., Gilewicz, M. and Bertrand, J.C. (1992) Effect of oxygen on *Pseudomonas nautica* growth on n-alkane with and without nitrate. Arch Microbiol 157, 538-545.

Brindle, K., Stephenson, T. and Semmens, M.J. (1998) Nitrification and oxygen utilisation in a membrane aeration bioreactor. J Membr Sci 144(1-2), 197-209.

Bueno, E., Mania, D., Frostegard, A., Bedmar, E.J., Bakken, L.R. and Delgado, M.J. (2015) Anoxic growth of Ensifer meliloti 1021 by N_2O-reduction, a potential mitigation strategy. Front Microbiol 6, 537.

Caporaso, J.G., Kuczynski, J., Stombaugh, J., Bittinger, K., Bushman, F.D., Costello, E.K., Fierer,

442 N., Pena, A.G., Goodrich, J.K., Gordon, J.I., Huttley, G.A., Kelley, S.T., Knights, D., Koenig,
443 J.E., Ley, R.E., Lozupone, C.A., McDonald, D., Muegge, B.D., Pirrung, M., Reeder, J.,
444 Sevinsky, J.R., Turnbaugh, P.J., Walters, W.A., Widmann, J., Yatsunenko, T., Zaneveld, J. and
445 Knight, R. (2010) QIIME allows analysis of high-throughput community sequencing data.
446 Nature Methods 7(5), 335-336.

447 Chang, C.Y., Tanong, K., Xu, J. and Shon, H. (2011) Microbial community analysis of an aerobic
448 nitrifying-denitrifying MBR treating ABS resin wastewater. Bioresour Technol 102(9),
449 5337-5344

450 Chèneby, D., Hartman, A., Hernault, C., Topp, E. and Germon, J.C. (1998) Diversity of denitrifying
451 microflora and ability to reduce N_2O in two soils. Biol Fertil Soils 28, 19-26.

452 Cole, A.C., Semmens, M.J. and LaPara, T.M. (2004) Stratification of activity and bacterial
453 community structure in biofilms grown on membranes transferring oxygen. Appl Environ
454 Microbiol 70(4), 1982-1989.

455 Cole, A.C., Shanahan, J.W., Semmens, M. and LaPara, T.M. (2002) Preliminary studies on the
456 microbial community structure of membrane-aerated biofilms treating municipal wastewater.
457 Desalination 146, 421-426.

458 Daelman, M.R.J., van Voorthuizen, E.M., van Dongen, L.G.J.M., Volcke, E.I.P. and van Loosdrecht,
459 M.C.M. (2013) Methane and nitrous oxide emission from municipal wastwater treatment-
460 results from a long term study. Water Sci Technol. 67(10), 2350-2359.

461 Desloover, J., Roobroeck, D., Heylen, K., Puig, S., Boeckx, P., Verstraete, W. and Boon, N. (2014)
462 Pathway of nitrous oxide consumption in isolated Pseudomonas stutzeri strains under anoxic
463 and oxic conditions. Environ Microbiol 16(10), 3143-3152.

464 Desloover, J., Vlaeminck, S.E., Clauwaert, P., Verstraete, W. and Boon, N. (2012) Strategies to
465 mitigate N_2O emissions from biological nitrogen removal systems. Curr Opin Biotechnol 23(3),

474-482.

Domingo-Félez, C., Mutlu, A.G., Jensen, M.M. and Smets, B.F. (2014) Aeration strategies to mitigate nitrous oxide emissions from single-stage nitritation/anammox reactors. Environ Sci Technol 48(15), 8679-8687.

Downing, L.S. and Nerenberg, R. (2007) Performance and microbial ecology of the hybrid membrane biofilm process for concurrent nitrification and denitrification of wastewater. Water Sci Technol 55(8-9), 355.

Downing, L.S. and Nerenberg, R. (2008a) Effect of bulk liquid BOD concentration on activity and microbial community structure of a nitrifying, membrane-aerated biofilm. Appl Microbiol Biotechnol 81(1), 153-162.

Downing, L.S. and Nerenberg, R. (2008b) Total nitrogen removal in a hybrid, membrane-aerated activated sludge process. Water Res 42(14), 3697-3708.

Etchebehere, C. and Tiedje, J. (2005) Presence of two different active nirS nitrite reductase genes in a denitrifying Thauera sp. from a high-nitrate-removal-rate reactor. Appl Environ Microbiol 71(9), 5642-5645.

Finkmann, W., Altendorf, K., Stackebrandt, E. and Lipski, A. (2000) Characterization of N_2O-producing Xanthomonas-like isolates from biofilters as *Stenotrophomonas nitritireducens sp. nov.*, *Luteimonas mephitis gen. nov., sp. nov.* and *Pseudoxanthomonas broegbernensis gen. nov.,sp. nov.* Int J Syst Evol Microbiol 50, 273-282.

Gabarro, J., Hernandez-Del Amo, E., Gich, F., Ruscalleda, M., Balaguer, M.D. and Colprim, J. (2013) Nitrous oxide reduction genetic potential from the microbial community of an intermittently aerated partial nitritation SBR treating mature landfill leachate. Water Res 47(19), 7066-7077.

Hsieh, Y. L., Tseng, S.K. and Chang, Y. J. (2002) Nitrification using polyvinyl alcohol-immobilized

nitrifying biofilm on an O2-enriching membrane. Biotechnol Lett 24, 315–319.

IPCC (2007) Summary for Policy-makers, Climate Change 2007: Mitigation. Contribution of Working Group III to the Fourth Assessment Report of the IPCC. In B. Metz, O.R. Davidson, P.R. Bosch, R. dave, L.A. Meyer eds. . Cambridge University Press, Cambridge, United Kingdom and New York, NY, USA.

Itoh, H., Navarro, R., Takeshita, K., Tago, K., Hayatsu, M., Hori, T. and Kikuchi, Y. (2014) Bacterial population succession and adaptation affected by insecticide application and soil spraying history. Front Microbiol 5(457), 1-12.

Itokawa, H., Hanaki, K. and Matsuo, T. (2001) Nitrous oxide production in high-loading biological nitrogen removal process under low COD/N ratio condition. Water Res 35(3), 657-664.

Jones, C.M., Graf, D.R., Bru, D., Philippot, L. and Hallin, S. (2013) The unaccounted yet abundant nitrous oxide-reducing microbial community: a potential nitrous oxide sink. ISME J 7(2), 417-426.

Jones, C.M., Stres, B., Rosenquist, M. and Hallin, S. (2008) Phylogenetic analysis of nitrite, nitric oxide, and nitrous oxide respiratory enzymes reveal a complex evolutionary history for denitrification. Mol Biol Evol 25(9), 1955-1966.

Kampschreur, M.J., Temmink, H., Kleerebezem, R., Jetten, M.S. and van Loosdrecht, M.C. (2009) Nitrous oxide emission during wastewater treatment. Water Res 43(17), 4093-4103.

LaPara, T.M., Cole, A.C., Shanahan, J.W. and Semmens, M.J. (2006) The effects of organic carbon, ammoniacal-nitrogen, and oxygen partial pressure on the stratification of membrane-aerated biofilms. J Ind Microbiol Biotechnol 33(4), 315-323.

Law, Y., Ye, L., Pan, Y. and Yuan, Z. (2012) Nitrous oxide emissions from wastewater treatment processes. Philos Trans R Soc Lond B (367), 1265-1277.

Liu, B., Mao, Y., Bergaust, L., Bakken, L.R. and Frostegard, A. (2013) Strains in the genus *Thauera*

514 exhibit remarkably different denitrification regulatory phenotypes. Environ Microbiol 15(10),
515 2816-2828.
516 Liu, H., Yang, F., Wang, T., Liu, Q. and Hu, S. (2007) Carbon membrane-aerated biofilm reactor for
517 synthetic wastewater treatment. Bioprocess Biosyst Eng 30(4), 217-224.
518 Lorenzen, J., Larsen, L.H., Kjaer, T. and Revsbech, N. (1999) Biosensor determination of the
519 microscale distribution of nitrate, nitrate assimilation, nitrification, and denitrification in a
520 diatom-inhabited freshwater sediment. Appl Environ Microbiol 64(9), 3264-3269.
521 Matsumoto, S., Terada, A. and Tsuneda, S. (2007) Modeling of membrane-aerated biofilm: Effects
522 of C/N ratio, biofilm thickness and surface loading of oxygen on feasibility of simultaneous
523 nitrification and denitrification. Biochem Eng J 37(1), 98-107.
524 Morley, N. and Baggs, E.M. (2010) Carbon and oxygen controls on N_2O and N_2 production during
525 nitrate reduction. Soil Biol Biochem 42(10), 1864-1871.
526 Nerenberg, R. (2016) The membrane-biofilm reactor (MBfR) as a counter-diffusional biofilm
527 process. Curr Opin Biotechnol 38, 131-136.
528 Okabe, S., Oshiki, M., Takahashi, Y. and Satoh, H. (2011) N_2O emission from a partial
529 nitrification-anammox process and identification of a key biological process of N_2O emission
530 from anammox granules. Water Res 45(19), 6461-6470.
531 Pan, Y., Ni, B.J., Bond, P.L., Ye, L. and Yuan, Z. (2013) Electron competition among nitrogen
532 oxides reduction during methanol-utilizing denitrification in wastewater treatment. Water Res
533 47(10), 3273-3281.
534 Pellicer-Nacher, C., Sun, S., Lackner, S., Terada A., Schreiber, F. and Smets, B. (2010) Sequential
535 aeration of membrane-aerated biofilm reactors for high-rate autotrophic nitrogen removal:
536 experimental demonstration. Environ. Sci. Technol. 44, 7628-7634.
537 Peng, L., Ni, B.J., Erler, D., Ye, L. and Yuan, Z. (2014) The effect of dissolved oxygen on N_2O

production by ammonia-oxidizing bacteria in an enriched nitrifying sludge. Water Res 66, 12-21.

Philippot, L. (2002) Denitrifying genes in bacterial and Archaeal genomes. Biochimica et Biophysica Acta 1577, 355-376.

Robertson, G.P. and Groffman, P.M. (2015) Nitrogen transformations. In B. Metz, O.R. Davidson, P.R. Bosch, R. dave, L.A. Meyer eds. Cambridge E. A. Paul, editor. Soil microbiology, ecology and biochemistry. 4th edition. Academic Press, 421-446.

Rochette, P. and Janzen, H.H. (2005) Towards a revised coefficient for estimating N_2O emissions from legumes. Nutr Cycl Agroecosys 73(2-3), 171-179.

Rodriguez-Caballero, A., Aymerich, I., Marques, R., Poch, M. and Pijuan, M. (2015) Minimizing N_2O emissions and carbon footprint on a full-scale activated sludge sequencing batch reactor. Water Res 71, 1-10.

Sanford, R.A., Wagner, D.D., Wu, Q., Chee-Sanford, J.C., Thomas, S.H., Cruz-Garcia, C., Rodriguez, G., Massol-Deya, A., Krishnani, K.K., Ritalahti, K.M., Nissen, S., Konstantinidis, K.T. and Loffler, F.E. (2012) Unexpected nondenitrifier nitrous oxide reductase gene diversity and abundance in soils. Proc Natl Acad Sci USA 109(48), 19709-19714.

Schloss, P.D., Westcott, S.L., Ryabin, T., Hall, J.R., Hartmann, M., Hollister, E.B., Lesniewski, R.A., Oakley, B.B., Parks, D.H., Robinson, C.J., Sahl, J.W., Stres, B., Thallinger, G.G., Van Horn, D.J. and Weber, C.F. (2009) Introducing mothur: open-source, platform-independent, community-supported software for describing and comparing microbial communities. Appl Environ Microbiol 75(23), 7537-7541.

Scholten, T., Lukow, T., Auling, G., Kroppenstedt, M., Rainey, F.A. and Deikmann, H. (1999) *Thauera mechernichensis sp nov.*, an aerobic denitrifier from a leachate treatment plant. Int J Syst Bacteriol 49, 1045–1051.

562 Schreiber, F., Loeffler, B., Polerecky, L., Kuypers, M.M. and de Beer, D. (2009) Mechanisms of
563 transient nitric oxide and nitrous oxide production in a complex biofilm. ISME J 3(11),
564 1301-1313.
565 Schreiber, F., Wunderlin, P., Udert, K.M. and Wells, G.F. (2012) Nitric oxide and nitrous oxide
566 turnover in natural and engineered microbial communities: biological pathways, chemical
567 reactions, and novel technologies. Front Microbiol 3, 372.
568 Schulthess, R.V. and Gujer, W. (1996) Release of nitrous oxide (N_2O) from denitrifying activated
569 sludge: verification and application of a mathematical model. Water Res 30(3), 521-530.
570 Schweitzer, B., Huber, I., Amann, R., Ludwig, W. and Simon, M. (2001) Alpha- and
571 beta-Proteobacteria control the consumption and release of amino acids on lake snow
572 aggregates. Appl Environ Microbiol 67(2), 632-645.
573 Semmens, M.J., Dahm, K., Shanahan, J. and Christianson, A. (2003) COD and nitrogen removal by
574 biofilms growing on gas permeable membranes. Water Res 37(18), 4343-4350.
575 Song, K., Suenaga, T., Harper, W.F., Jr., Hori, T., Riya, S., Hosomi, M. and Terada, A. (2015)
576 Effects of aeration and internal recycle flow on nitrous oxide emissions from a modified
577 Ludzak-Ettinger process fed with glycerol. Environ Sci Pollut Res 22(24), 19562-19570.
578 Srinandan, C.S., Shah, M., Patel, B. and Nerurkar, A.S. (2011) Assessment of denitrifying bacterial
579 composition in activated sludge. Bioresour Technol 102(20), 9481-9489.
580 Stein, L.Y. and Klotz, M.G. (2011) Nitrifying and denitrifying pathways of methanotrophic bacteria.
581 Biochem Soc Trans 39(6), 1826-1831.
582 Suzuki, Y., Hatano, N., Ito, S. and Ikeda, H. (2000) Performance of nitrogen removal and biofilm
583 structure of porous gas permeable membrane reactor. Water Sci Technol 41(4-5), 211-217.
584 Syron, E. and Casey, E. (2008) Membrane-aerated biofilms for high rate biotreatment: performance
585 appraisal, engineering principles, scale-up, and development requirements. Environ Sci Technol

42(6), 1833-1844.

Syron, E., Semmens, M.J. and Casey, E. (2015) Performance analysis of a pilot-scale membrane aerated biofilm reactor for the treatment of landfill leachate. Chem Eng J 273, 120-129.

Tallec, G., Garnier, J., Billen, G. and Gousailles, M. (2006a) Nitrous oxide emissions from secondary activated sludge in nitrifying conditions of urban wastewater treatment plants: effect of oxygenation level. Water Res 40(15), 2972-2980.

Tallec, G., Garnier, J. and Gousailles, M. (2006b) Nitrogen removal in a wastewater treatment plant through biofilters: nitrous oxide emissions during nitrification and denitrification. Bioprocess Biosyst Eng 29(5-6), 323-333.

Tenno, T., Zekker, I., Rikmann, E., Tenno, T., Daija, L. and Mashirin, A. (2016) Modelling equilibrium distribution of carbonaceous ions and molecules in a heterogeneous system of $CaCO_3$–water–gas. P Est Acad Sci 65(1), 68.

Terada, A., Hibiya, K., Nagai, J., Tsuneda, S. and Hirata, A. (2003) Nitrogen removal characteristics and biofilm analysis of a membrane-aerated biofilm reactor applicable to high-strength nitrogenous wastewater treatment. J Biosci Bioeng 95(2), 170-178.

Terada, A., Sugawara, S., Yamamoto, T., Zhou, S., Koba, K. and Hosomi, M. (2013) Physiological characteristics of predominant ammonia-oxidizing bacteria enriched from bioreactors with different influent supply regimes. Biochem Eng J 79, 153-161.

Terada, A., Lackner, S., Kristensen, K. and Smets, B.F. (2010) Inoculum effects on community composition and nitritation performance of autotrophic nitrifying biofilm reactors with counter-diffusion geometry. Environ Microbiol 12(10), 2858-2872.

Walter, B., Haase, C. and Rabiger, N. (2005) Combined nitrification/denitrification in a membrane reactor. Water Res 39(13), 2781-2788.

Wang, Z., Zhang, X., Lu, X., Liu, B., Li, Y., Long, C. and Li, A. (2014) Abundance and diversity of

bacterial nitrifiers and denitrifiers and their functional genes in tannery wastewater treatment plants revealed by high-throughput sequencing. PLoS One 9(11), 1-19.

Wrage, N., Velthol, G.L., Beusichem, M.L. and Oenema, O. (2001) Role of nitrifier denitrification in the production of nitrous oxide. Soil Biol Biochem 33, 1723-1732.

Wunderlin, P., Mohn, J., Joss, A., Emmenegger, L. and Siegrist, H. (2012) Mechanisms of N_2O production in biological wastewater treatment under nitrifying and denitrifying conditions. Water Res 46(4), 1027-1037.

Yokoyama K, Yumura M, Honda T, Ajitomi E (2016) Characterization of denitrification and net N_2O-reduction properties of novel aerobically N_2O-reducing bacteria. Soil Sci Plant Nutr 62, 230-239.

Yoon, S., Nissen, S., Park, D., Sanford, R.A. and Loffler, F.E. (2016) Nitrous oxide reduction kinetics distinguish bacteria harboring clade I versus clade II NosZ. Appl Environ Microbiol 82(13), 3793-3800.

Yu, I.S., Yeom, S.J., Kim, H.J., Lee, J.K., Kim, Y.H. and Oh, D.K. (2008) Substrate specificity of Stenotrophomonas nitritireducens in the hydroxylation of unsaturated fatty acid. Appl Microbiol Biotechnol 78(1), 157-163.

Zhao, Y., Huang, J., Zhao, H. and Yang, H. (2013) Microbial community and N removal of aerobic granular sludge at high COD and N loading rates. Bioresour Technol 143, 439-446.

Zumft, W. (1997) Cell biology and molecular basis of denitrification. Microbiol Mol Biol Rev 61(4), 533-616.

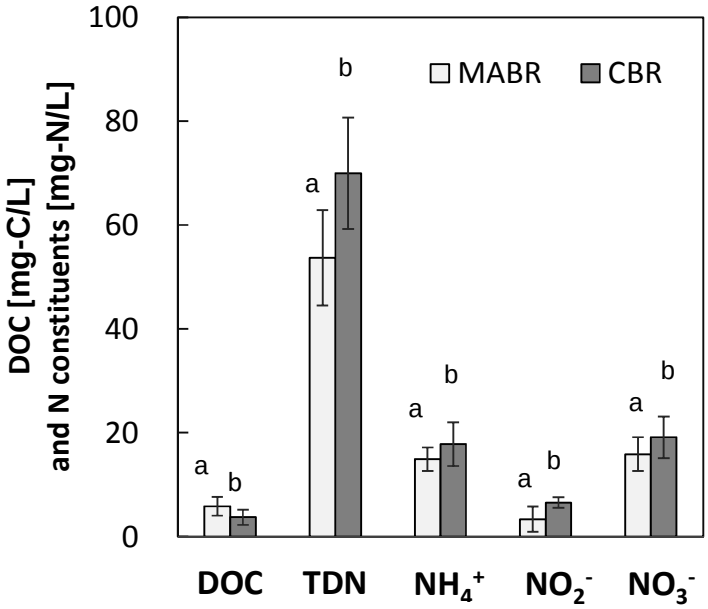

Figure 1. Average concentrations in effluent of dissolved organic carbon (DOC), total dissolved nitrogen (TDN), ammonium (NH_4^+), nitrite (NO_2^-), and nitrate (NO_3^-) in the steady state (day 43–95) in the MABR and CBR. Different letters for each constituent indicate a significant difference ($p < 0.05$) between the MABR and CBR.

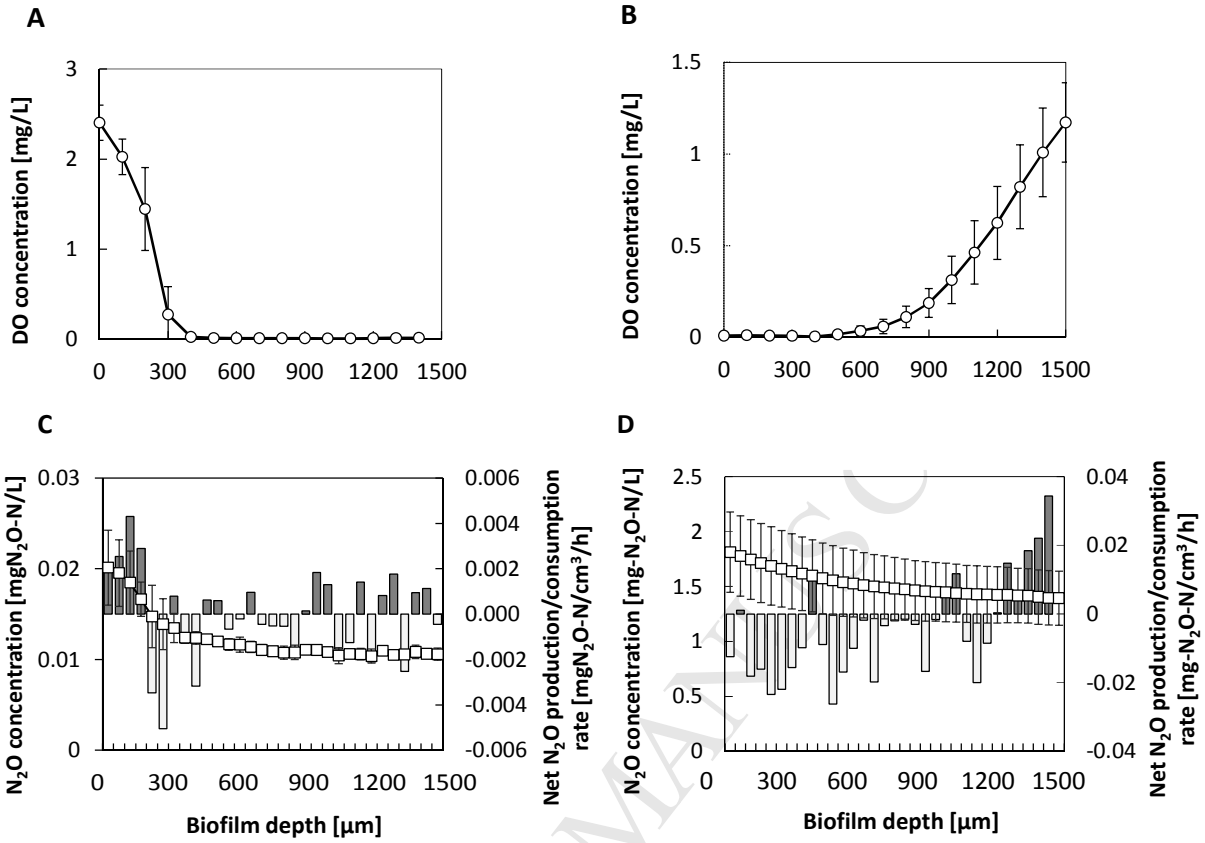

Figure 2. Depth profiles of O_2 and N_2O concentrations and average net N_2O production/consumption rates (bar charts) in the MABR biofilm (A: DO profile; C: N_2O profile) and CBR biofilm (B: DO profile; C: N_2O profile). Note that net N_2O production (positive value) and consumption (negative value) rates (g-N/cm^3/h) are based on biofilm volume. The measurement was carried out during operation days 90–95. The point at 0 µm represents the biofilm base.

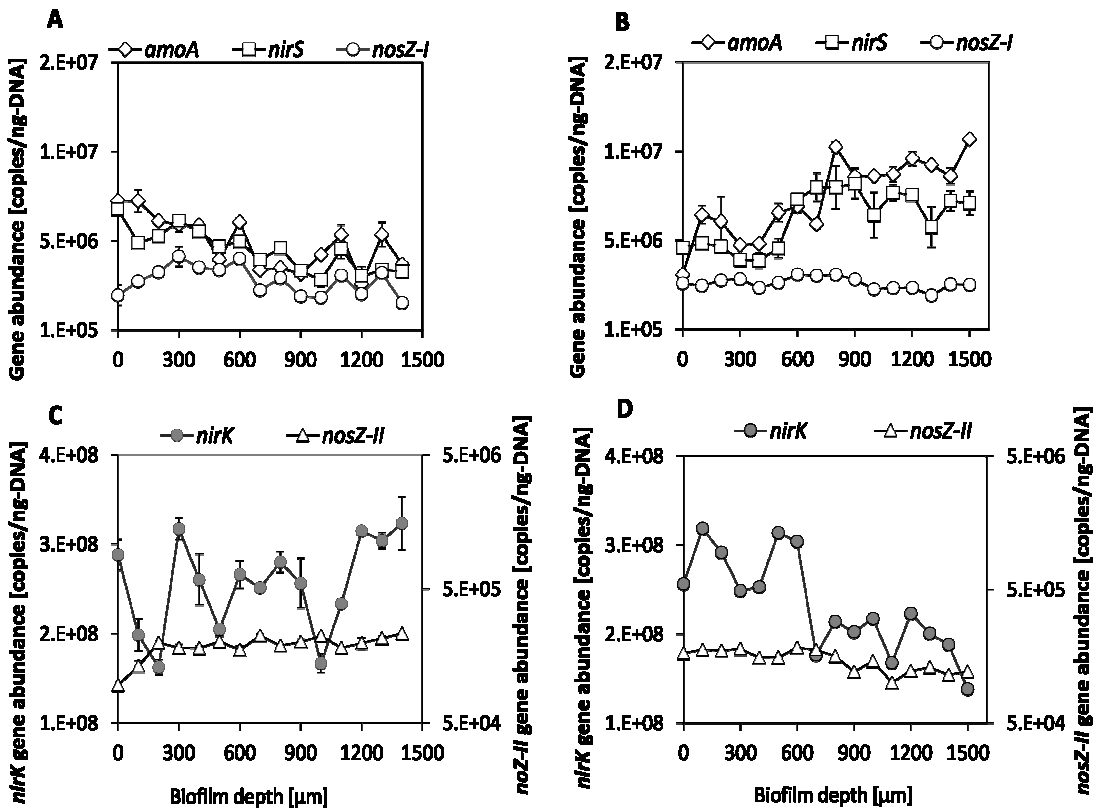

Figure 3. Depth profiles of functional genes for AOB (*amoA*) and denitrification (*nirS*, *nirK*, clade I *nosZ*, and clade II *nosZ*) in the biofilms of the MABR (A and C) and CBR (B and D). The point at 0 µm represents the biofilm base.

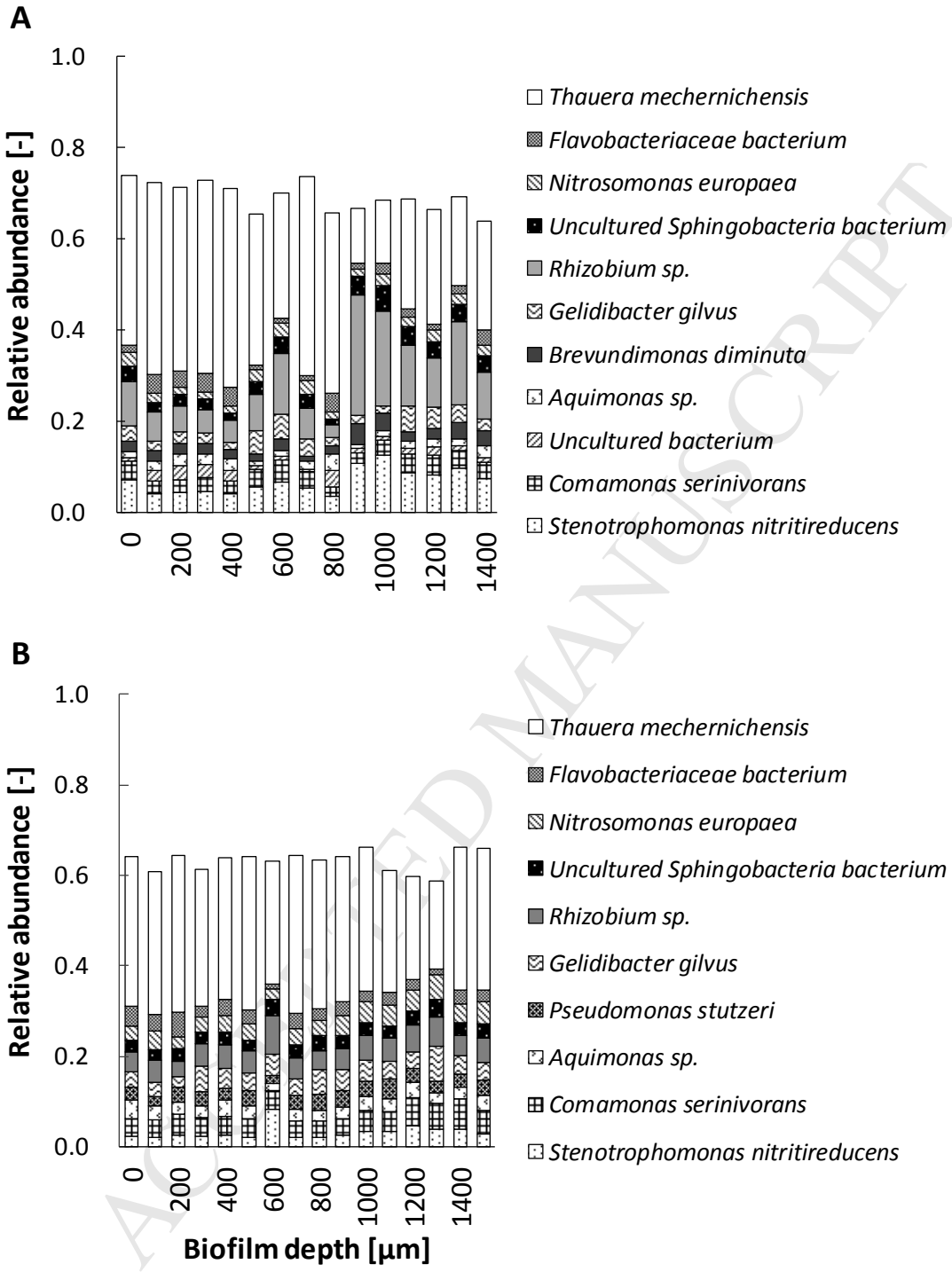

Figure 4. Depth-profile of relative bacterial abundance at the OTU level in the biofilms of the MABR (A) and CBR (B). All OTUs detected at least in one biofilm depth at ≥3% relative abundance are shown. The point at 0 µm represents the biofilm base.

Highlights

- Depth profiles of N_2O and microbial community were compared between a MABR and CBR.
- Dissolved N_2O level was two orders of magnitude lower in the MABR than the CBR.
- Zones for N_2O production and consumption were close together in the MABR biofilm.
- Key N_2O-reducing bacteria, which may contribute to N_2O mitigation, were identified.